Unexpected kinetic behavior of structured Pd/CeO2–ZrO2 toward undesired ammonia formation and consumption during nitrites reduction: Role of the reactivity of oxygen from ceria

Jean-Philippe Dacquin, S. Troncéa, V.I. Parvulescu, Pascal Granger

Submitted to a special issue of the journal Catalysis Today entitled ***"Structured and micro-structured catalysts : a fascinating future for a sustainable world"*** in honor of Profs. Jové Antonio Odriozola and Mario Montes on their 65th birthday
Manuscript ID : CATTOD-D-20-00238

Unexpected kinetic behavior of structured Pd/CeO_2-ZrO_2 towards undesired ammonia formation and consumption during nitrites reduction : Role of the reactivity of oxygen from ceria

J.P. Dacquin,[1*] S. Troncéa,[1,2] V.I. Parvulescu,[2*] P. Granger,[1*]

[1] *Univ. Lille, CNRS, Centrale Lille, ENSCL, Univ. Artois, UMR 8181 - UCCS - Unité de Catalyse et Chimie du Solide, F-59000 Lille, France*
[2] *University of Bucharest, Department of Organic Chemistry, Biochemistry and Catalysis, B-dul Regina Elisabeta 4-12, Bucharest 030016, Romania.*

Corresponding authors :
Prof. Pascal Granger
Email. : pascal.granger@univ-lille.fr
Phone number : +33 320434938

Dr. Jean-Philippe Dacquin
Email. : jean-philippe.dacquin@univ-lille.fr
Phone number : +33 320434795

Prof. Vasile I. Parvulescu
Email. : vasile.parvulescu@chimie.unibuc.ro
Phone number : +40 214100241

Abstract

This study deals with the kinetics of successive ammonia production and unexpected consumption in the course of the catalytic water denitrification over $Pd/Ce_xZr_{1-x}O_2$ catalysts. A fast conversion of nitrites to ammonium ions was found weakly dependent of the particle size of palladium likely due to the juxtaposition of electronic effects stabilizing electron-rich Pd active sites more prone to produce ammonia instead of nitrogen. Subsequent slow consumption of ammonia in anaerobic conditions occurred on $Pd/Ce_xZr_{1-x}O_2$ whereas Pd/ZrO_2 was found inactive for this sequential reaction. Kinetic measurements from semi batch experiments led to the estimation of rate constants. Particular attention was paid to ammonia oxidation reaction with a pseudo rate constant depending on the surface coverage of reactive oxygen from ceria then revealing the importance of the synthesis route of $Ce_xZr_{1-x}O_2$ and peculiar interaction with Pd.

Keywords : Catalytic reduction of nitrites, water denitrification, ammonia, palladium, ceria-zirconia mixed oxides.

1. Introduction

More stringent standard regulations set at the European level concern soluble N-containing species in drinking water [1]. Presently, current biological and physicochemical treatments are implemented but exhibiting several economic and ecological disadvantages [2]. Catalytic processes could represent a valuable alternative using hydrogen as a green reducing agent [2]. However, because of the undesired production of ammonia, a future up-scaling must face important technical issues regarding the catalyst stability and selectivity. In practice, this goal was achieved by a combination of catalysis and ion exchange that can lead to a complete removal of ammonium ions [3].

The reduction of nitrates involves consecutive and parallel reactions [4]. Nitrates are intermediately reduced to nitrites and further converted to gaseous nitrogen. The formation of ammonia is also occurring during this process. Therefore, to avoid adverse health effects, its formation must be limited to a maximum concentration fixed by the legislation at 0.5 mg/L. A complete reduction of nitrates to nitrogen is generally achieved on bimetallic catalysts especially when palladium is combined with copper [5-7]. Both metals cooperate with copper catalyzing the reduction of nitrates to nitrites and palladium converting nitrites to nitrogen.

Earlier investigations searching for the influence of the size and morphology of supported metallic nanosized Pd particles recognized the structure-sensitivity of the hydrogenation of nitrates to nitrogen [8]. Nevertheless, the kinetic behavior can be more complex when reducible materials are used as support, such as CeO_2, because the reduction of nitrates to nitrogen would involve oxygen vacancies as reported elsewhere [9]. The preservation of the metallic character has been found as a crucial parameter in the course of the reaction which could distort any conclusion related to the structure-sensitivity. Indeed, Kim et al. [10] concluded that an improved activity is attributable to the reduced surface of the support and

the zero-valent active metal. More recently, transient kinetic experiments coupled to *in situ* infrared spectroscopic measurements led to divergent conclusions related the composition of the active sites involving the metal-support interaction and the presence of partially oxidized Pd species [11] instead of single metallic sites. All these observations do not emphasize a clear consensus likely due to the fact that geometric and electronic effects are usually difficult to differentiate.

Based on this state of the art, this present study was devoted to the second step, i.e. to that associated to the reduction of nitrites by gaseous hydrogen on Pd/CeO_2-ZrO_2. Previous investigations revealed the occurrence of the deactivation through particle sintering and a partial loss of metallic character through an oxidation in the aqueous phase [12]. The creation of strong-metal support interactions on reducible support materials can stabilize more active electron-rich metallic particles. However, a careful monitoring of the electron transfer is mandatory to prevent over hydrogenation processes leading inevitably to the production of ammonia at the expense of nitrogen.

Recently, we showed the advantages provided by the elaboration of CeO_2-ZrO_2 mixed oxides according to a soft templating method such as evaporation induced self-assembly (EISA) compared to a conventional co-precipitation route [13,14]. The most promising catalytic performances were observed on low loaded Pd samples dispersed on CeO_2-ZrO_2 prepared by the EISA method. These demonstrate preferential interactions of Pd with the tetragonal structure of the solid solutions [14]. It was also found that this peculiar interaction can originate a secondary ammonia oxidation reaction to nitrogen whereas the re-oxidation to nitrites would take place more significantly on Pd supported on CeO_2-ZrO_2 prepared by co-precipitation.

Up to now, such a behavior has not been extensively reported in the literature especially under anaerobic conditions where the hypothesis of a direct involvement of the surface oxygen from

ceria in an ammonia re-oxidation process can be demonstrated [13,14]. Based on this, this study proposes a kinetic approach to understand more accurately the intrinsic reactivity of surface oxygen species depending on the preparation route of the support material and its specific interaction with palladium which could be involved in the sequential process.

2. Experimental

$Ce_xZr_{1-x}O_2$ was prepared through i) a sol-gel method combined with evaporation-induced self-assembly (EISA) process in ethanol using block copolymer Pluronic P123 as template and cerium nitrate and zirconium oxychloride as precursor salts [9] and ii) a conventional co-precipitation method (COP) using $Ce(NO_3)_3.6H_2O$ and $ZrOCl_2 \cdot 8H_2O$ as precursor salts dissolved in aqueous phase. Oxy-hydroxides were precipitated by adding drop-wise ammonia. In the EISA approach, the solvent evaporation was carried out in a climate chamber under air humidity and the drying step was performed following the already reported single and two-steps procedures [14]. The dried samples were then calcined in air at 400°C for 4 hours. The supported Pd catalysts containing 2.3 or 0.46 wt.% Pd were prepared by incipient wetness impregnation. Dried precursors were calcined in air at 400°C and then, *ex situ* reduced in pure hydrogen at 300°C or 500°C.

The specific surface area (SSA) was determined from nitrogen physisorption measurements at -196°C on a Micrometrics Tristar 3020 analyzer according to the BET equation. Hydrogen chemisorption measurements were carried out at 100°C on a Micromeritics Autochem II 2920 apparatus on samples pre-reduced at 300 or 500°C under a flow of 20 mL/min of pure hydrogen and then evacuated in Ar at the selected temperature. H_2 pulses where injected until saturation and Pd dispersion was calculated according to the stoichiometric ratio H/Pd = 1. XPS measurements were performed an AXIS Ultra DLD Kratos spectrometer equipped with a

monochromatized aluminum source for excitation (1486.6 eV). C 1s core level at 284.8 eV served as internal reference for the correction of Binding Energy (B.E.) values.

The nitrite reduction reaction was performed in a 250 mL semi batch glass made reactor at atmospheric pressure. 80 or 400 mg of powder catalyst with respective palladium loading of 2.3 and 0.46 wt.% and an average grain size of 250 μm, were firstly introduced in the reactor and then exposed to a flow of H_2 for 1 hour at room temperature (RT). In the second stage, 40 mL of degassed ultrapure water was added to the system under a flow of H_2 (200 mL/min) for 1 hour. Afterwards, 10 mL of nitrites solution (500 mg/L) were introduced and the suspension was stirred with a rotation speed set at 700 rpm insuring the absence of any significant external mass transfer phenomena [9]. All catalytic testings were performed using the same initial nitrites concentration of 2.2 mmol/L and taking the same amount of palladium in the batch reactor equivalent to 17.3 μmol Pd into account. Nitrite and ammonia concentration was monitored by an ionic chromatograph: Metrohm 844 UV/VIS and Metrohm 861 Advanced Compact respectively.

3. Results and discussion

3.1. Physicochemical characterization of supported Pd on ceria-zirconia mixed oxides, CeO_2 and ZrO_2 single oxides

Bulk characterization has been earlier discussed [14]. Particular attention was paid in this study to the impact of the solvent evaporation and drying upon the textural and structural properties of the CZ(EISA) samples. These are preliminary steps prior the calcination in air. The values collected in Table S1 in the Supplementary Materials correspond to samples dried in air in a single step at 60 or 100°C and in a two-steps process at the same temperatures. This comparison shows that the best compromise in terms of specific surface area (SSA), total pore

volume and average pore size diameter is obtained after drying at 100°C. Indeed, while a slightly smaller value of the SSA is obtained for the sample dried at 100°C, the formation of larger pores is an important criterion to improve the catalyst efficiency thanks to an enhanced speed up of the mass transfer phenomena.

Raman spectra are presented in Figs S1 (see Supplementary Materials). The assignments of signals confirm the stabilization of the tetragonal structure of $Ce_xZr_{1-x}O_2$ prepared by the EISA irrespective the drying conditions, i.e. single or two steps procedure. The dominant Raman line at 490 cm^{-1} is ascribed to the F2g mode for a cubic fluorite structure with a space group Fm3m. The intensity ratio of this line to that observed at 627 cm^{-1} (related to disturbances of the local M-O bond and the presence of oxygen vacancies in the ceria lattice [15]) is representative for the population of the oxygen vacancies. Qualitatively, a higher ratio corresponds to a larger stabilization of the anionic vacancies. This drying protocol has been further extended for Pd/CZ(EISA), CeO_2(EISA) and ZrO_2(EISA).

Textural properties of $Ce_xZr_{1-x}O_2$ prepared by the EISA and co-precipitation methods are presented in Table 1. They differ from those measured for single CeO_2 and ZrO_2 oxides especially through a significant enhancement of the surface area for mixed oxides. Such a behavior is usually related to the stabilization of the solid solutions and is caused by the insertion of zirconium in the fluorite structure of CeO_2 [16,17] and the sensibility of CeO_2 to the thermal sintering. The larger intensity of the 490 cm^{-1} Raman line (see Fig. S2 in Supplementary Materials) for CZ(COP) underlines a weaker ability to stabilize the anionic vacancies as aforementioned. Partial segregations leading to Ce-rich macro domains in CZ(COP) could also induce similar changes of the intensity ratio as it has previously been evidenced [14]. As a first approximation, the ability to stabilize a greater extent of anionic vacancies could be a key point for improving the dispersion and strengthening the Pd-Ce interaction.

Table 1. Elemental and textural analysis of $Ce_{0.5}Zr_{0.5}O_2$ prepared by coprecipitation and the EISA method.

Sample	Ce (at.%)	Zr (at.%)	Ce/(Ce+Zr)	Specific Surf. Area (m^2 g^{-1})	Total pore vol. (cm^3 g^{-1})	Average pore size (nm)
CZ(EISA)	0.35	0.65	0.35	90	0.13	5.7
CZ(COP)	0.43	0.57	0.43	100	0.10	6.5
CeO_2(EISA)				14	0.04	11.9
ZrO_2(EISA)				62	0.10	6.7

H_2 chemisorption measurements on pre-reduced samples at 300 and 500°C were performed at 100°C in order to avoid the bulk palladium hydride formation which would lead to an overestimation of the H_2 uptake. The estimates of Pd dispersion and average particle size, assuming a stoichiometry H/Pd = 1 and hemispherical particles, are collected in Table S2. Fig. 1 illustrates the impact of the reduction temperature and palladium loading on the Pd dispersion. An additional verification of these results was achieved from TEM measurements carried out on 2.3Pd/CZ(EISA) as illustrated in Fig. 2. The average Pd particle size was found around 8.0 nm that is close to that estimated from H_2 chemisorption (~6.1 nm) showing an acceptable consistency also suggesting the absence of any significant deviation caused by a H_2 uptake over-estimation.

These results also confirm that an increase of the pre-reduction temperature has a strong detrimental effect on the palladium dispersion irrespective of the support composition and is attributed to the sintering of particles at high temperature. Interestingly, the highest dispersion value is observed for 0.46Pd/CeO_2(EISA) reduced at 300°C despite the lowest specific surface area measured on CeO_2. Such a comparison suggests that the dispersion of Pd at low metal loadings could be more influenced by the support composition instead of its surface area, and especially by its ability to promote the formation of surface anionic vacancies thanks to a weakening of the Ce-O bond. A priori, the influence of the crystallographic phase upon

the oxygen mobility might influence the extent of the formation of the surface anionic vacancies that is more favorable for cubic CeO_2 than for tetragonal ZrO_2 and Zr-rich $Ce_xZr_{1-x}O_2$ mixed oxides [18]. While an increase in the palladium content induces a loss of Pd dispersion on CeO_2(EISA), the opposite tendency is noticeable on Pd/CZ and Pd/ZrO_2 samples. One can hypothesize that this unexpected trend, corresponding to a gain in dispersion with a rise in Pd content, could be jointly related to higher specific surface area and a larger fraction of more reducible oxidic Pd species compared to low loaded samples**.**

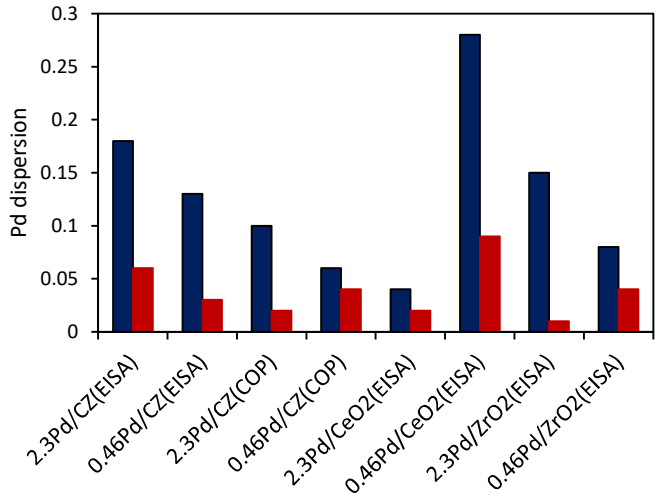

Fig. 1. The influence of the metal loading and pre-reduction temperature on the palladium dispersion on CZ(EISA) and CZ(COP) (in blue samples pre-reduced at 300°C; and red at 500°C).

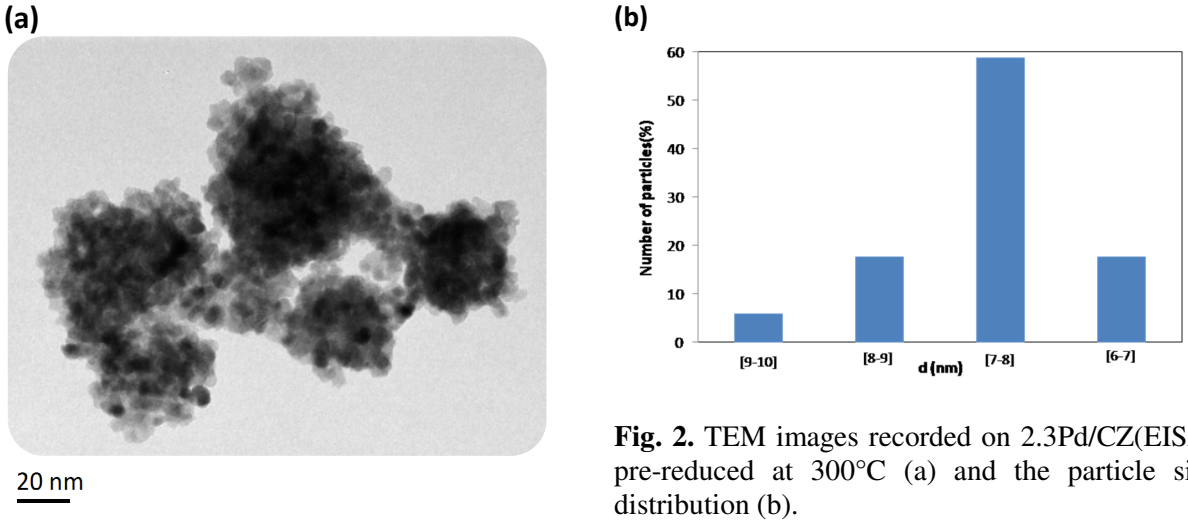

Fig. 2. TEM images recorded on 2.3Pd/CZ(EISA) pre-reduced at 300°C (a) and the particle size distribution (b).

XPS analysis were performed on calcined samples, providing complementary information on the surface elemental composition. These analyses for palladium supported on ceria-zirconia mixed oxide showed significant changes according to the utilized preparation method (EISA vs. co-precipitation) (Table 2). Binding energy values have been earlier discussed [14] and were not reported. They essentially characterize the presence of Zr^{4+}, Pd^{2+}, Ce^{4+} and Ce^{3+} in lesser extent as no *in situ* pre-treatment was performed prior XPS measurements. Let us note that B.E. values for Pd $3d_{5/2,}$ in the range 337.4-338.4 eV, exceed those currently reported for PdO (in between 336.1 and 336.9 eV) and could reflect the presence of well-dispersed PdO_x species in strong interaction with $Ce_xZr_{1-x}O_2$. More interesting is the distribution of these species at the outermost surface. Particular attention can be paid to the ratio Ce/(Ce+Zr), O/(Zr+Ce) and Ce^{3+}/Ce^{4+} since an increase in the Ce^{3+} concentration could be correlated to the formation of oxygen vacancies [19]. The values of the Ce/(Ce+Zr) ratio, varying the range 0.36-0.42 for Pd/CZ(EISA) are in concordance to elemental analysis (Table 1). However, strong deviations were observed for the Pd/CZ(COP) revealing a significant surface Ce enrichment. The evolutions observed for the O/(Ce+Zr) ratio indicate a higher surface oxygen concentration for Pd/CZ(COP) which could be in a good agreement with the observations previously discussed. The lower value measured for Pd/CZ(EISA) seems to be also in relative good agreement with previous Raman spectroscopic observations underlining a greater stabilization of anionic vacancies especially on 0.46Pd/CZ(EISA) exhibiting the highest Ce^{3+}/Ce^{4+} ratio. Significant evolutions are also observed on the Pd/(Ce+Zr) ratio. Probably the most relevant comparison comes from 0.46Pd/CZ(EISA) and 0.46Pd/CZ(COP). Despite the higher Pd concentration of the latter catalyst, the lower dispersion could reflect a weaker Pd-Ce interaction compared to 0.46Pd/CZ(EISA) thus, also explaining a greater sensitivity to sintering.

Table 2. XPS analysis on calcined Pd-doped $Ce_xZr_{1-x}O_2$.

Catalyst	Relative surface composition			
	Ce/(Ce+Zr)	Pd/(Ce+Zr)	O/(Ce+Zr)	Ce^{3+}/Ce^{4+}
0.46Pd/CZ(EISA)	0.36	0.70×10^{-2}	2.20	0.42
2.3Pd/CZ(EISA)	0.42	5.66×10^{-2}	2.34	0.29
0.46Pd/CZ(COP)	0.54	6.18×10^{-2}	2.81	0.21
2.3Pd/CZ(COP)	0.52	-	2.69	0.35

3.2. Kinetics of nitrites reduction and related production of ammonia

The kinetics of the overall reduction of nitrites on Pd supported on ceria-zirconia mixed oxide has been earlier reported [14]. Additional experiments were performed in batch conditions on Pd supported on single ZrO_2 and CeO_2 oxide materials to get more insights into the specific role played by the support composition which can modulate the strength of interactions with Pd particles and their related catalytic properties. Prior to kinetic exploitation and the calculation of initial specific rates and TOF values for nitrites reduction, an important question arises related to the limiting species that could determine the rate through an internal mass transport, where it could be gaseous hydrogen or nitrites. The detection of such limitations has not been apprehended according to an experimental approach bringing together three distinct phases: liquid/solid/gas. Regarding the complexity of such catalytic system the effective diffusivities of the different species and the presence of significant internal mass transfer limitations have been roughly estimated through the calculation of the Weisz Prater criterion according to Eq. (1).

$$\frac{r_{obs}\, L^2}{C_{obs,Ai}\, D_{eff,Ai}} < 1 \qquad (1),$$

where: r_{obs} - stands for the initial volumic rate (mol m^{-3} s^{-1}), $L = d_p/6$ - the volume to surface ratio of the grain in m, $C_{obs,Ai}$ - the initial concentration of the reactant A_i (mol m^{-3}), with A_i = NO_2^- or H_2 and $D_{eff,Ai}$ the effective diffusion (m^2 s^{-1}). Details on these calculations are reported in Supplementary Materials. The results obtained by considering the diffusion of nitrites

strictly fulfill the boundary conditions given by Eq. (1) suggesting that the chemical regime should prevail in a large extent. Similar calculations performed for H_2 diffusion, revealed numerical values for Eq. (1) slightly higher than 1 suggesting the occurrence of a mixed regime for high initial rate thus showing that mass transfer phenomena cannot be totally ruled out.

The initial specific rates expressed per gram of catalyst were calculated from the slope of the tangent at t = 0 of the concentration profiles of nitrites concentration vs. time. As seen in Fig. 3, a fast conversion of nitrites takes place at the early stage of the reaction on Pd/CZ(EISA) whereas slower conversions occur on Pd/CZ(COP). The related TOF values in Table 3, corresponding to a normalized rate expressed per surface Pd atom, were calculated based on the dispersion reported in Fig. 1 and Table S2 in Supplementary Materials. Particular attention was also paid to the evolution of ammonia concentration vs. time in Fig. 4 revealing different kinetic regimes related to an instant formation at the early stage of the reaction and a slower consumption of ammonia with a rise in nitrite conversion. Let's talk about the fast ammonia (stabilized as ammonium ions) production at the early stage of the reaction accompanied by a simultaneous slower production of nitrogen. As earlier explained [13], the initial product distribution reflects the structure sensitivity of this reaction, ammonia being formed on low coordinated Pd atoms on edge and corners of Pd particles with a distribution declining with a rise in Pd particle size. As a matter of fact, such a structure sensitivity can be regarded because two adjacent Pd atoms are requested for the recombination of two nitrogen atoms coming from the reduction of nitrites whereas only one is needed for its subsequent hydrogenation to ammonia.

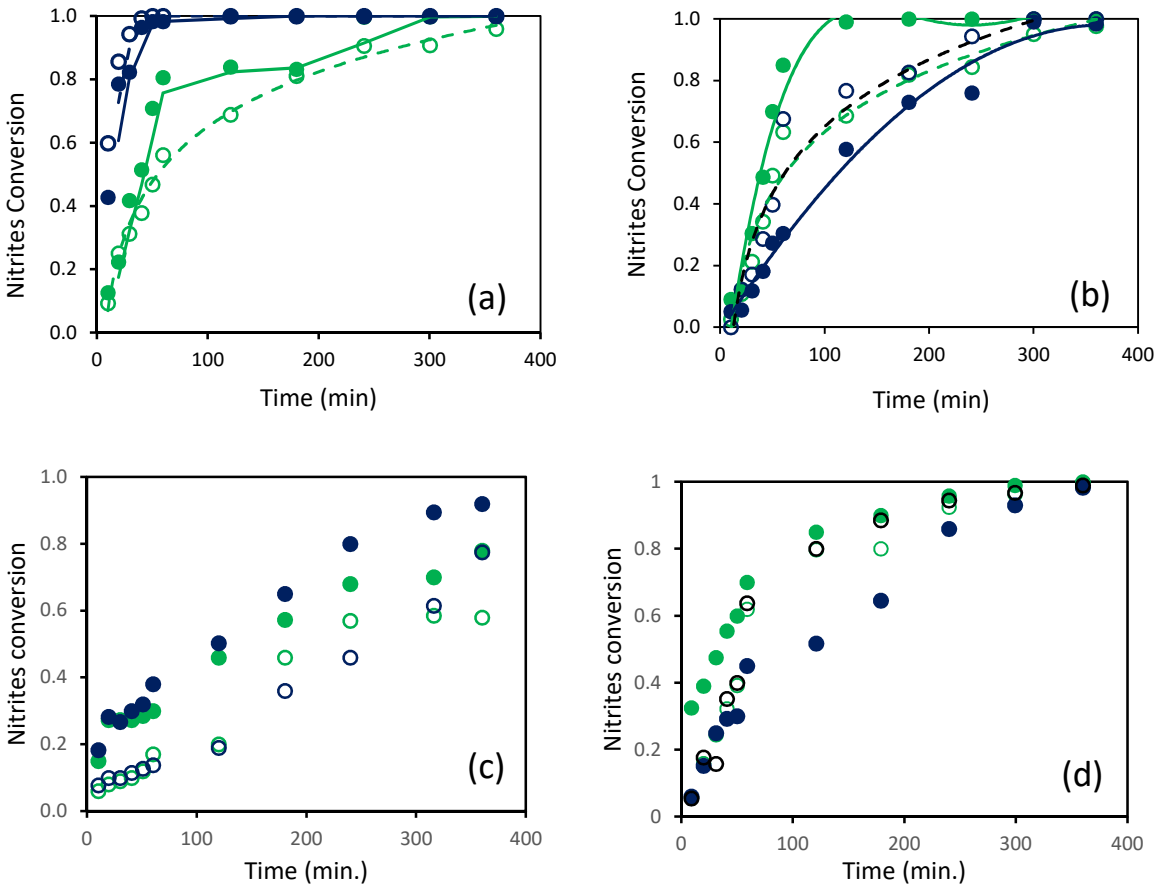

Fig. 3. Conversion profiles of nitrites ions vs. time during the reduction of nitrites by hydrogen in batch conditions with: (a) Pd/CZ(EISA), (b) Pd/CZ(COP), (c) Pd/ZrO_2(EISA), (d) Pd/CeO_2(EISA) ; full symbol corresponds to reduction at 300°C, open symbol to reduction at 500°C; 0.46 wt.% Pd in blue and 2.3 wt.% Pd in green.

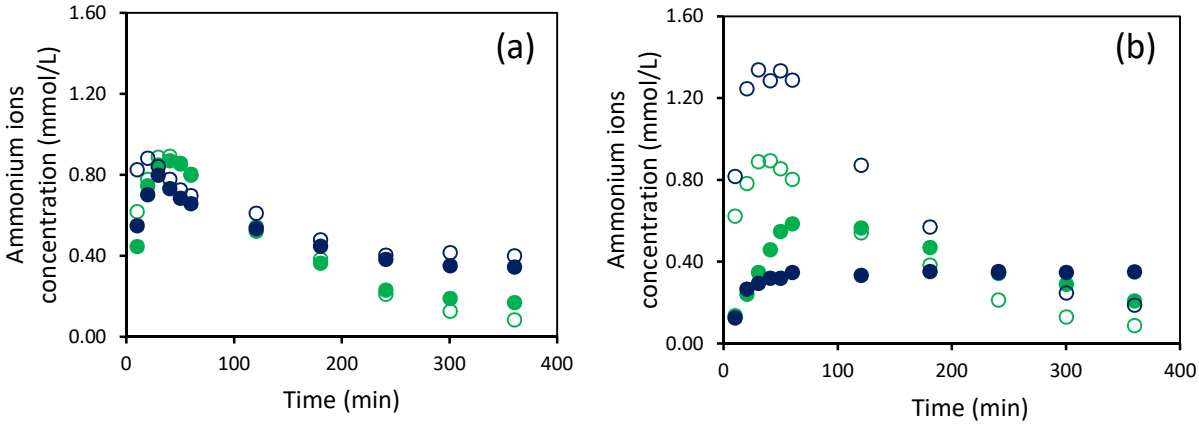

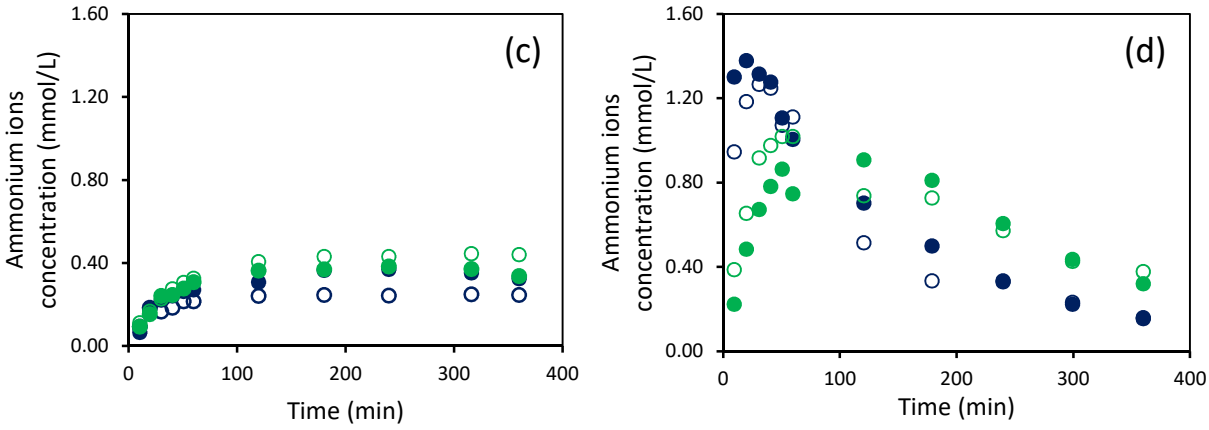

Fig. 4. Concentration profiles of ammonium ions vs. time formed during the reduction of nitrites by hydrogen in batch conditions with: (a) Pd/CZ(EISA), (b) Pd/CZ(COP), (c) Pd/ZrO_2(EISA), (d) Pd/CeO_2(EISA) ; full symbol corresponds to reduction at 300°C, open symbol to reduction at 500°C; 0.46 wt.% Pd in blue and 2.3 wt.% Pd in green.

Despite a significant dispersion of the TOF values, the plot of TOF vs. the particle size led to a particle size dependency of the rate as presented in Fig. 5. The much faster production of ammonia with lower structural requirements than that requested for nitrogen could partly buffer the size effect on TOF values explaining this dispersion. As a matter of fact, a more careful examination of Fig. 4 also indicates an important support effect on the catalytic properties of Pd particles towards the ammonia formation. As exemplified in Figs. 4(a) and (b), a weak reduction temperature dependency of ammonia production is discernible on Pd/CZ(EISA) contrarily to Pd/CZ(COP). It is worthwhile to note that Pd/CeO_2 mimics the behavior of Pd/CZ(COP) which emphasizes a significant impact of the support composition related to much stronger surface heterogeneities for CZ(COP). Indeed, CeO_2 or Ce-rich $Ce_xZr_{1-x}O_2$ solid solution coexists with the tetragonal Zr-rich $Ce_xZr_{1-x}O_2$ structure on CZ(COP) whereas the tetragonal structure predominates on CZ(EISA). This comparison suggests that a ligand effect could partly change the electronic structure of Pd particles in case of strengthening the metal-support interaction. Hence, the faster production of ammonia on Pd/CZ(COP) could be ascribed to a greater stabilization of electron-rich Pd particles more prone to promote an over-reduction of nitrites to ammonia, as reported elsewhere [20]. The

superposition of electronic induced effect through the use of reducible support makes the kinetic behavior more complex opening the discussion to an alternative single site reaction mechanism. Also, recent investigations suggested an alternative explanation with a dual site catalysis involving a preferential weak adsorption of nitrites on oxygen vacancies at the vicinity of Pd particles which are able to reduce these thanks to dissociated hydrogen atoms [21].

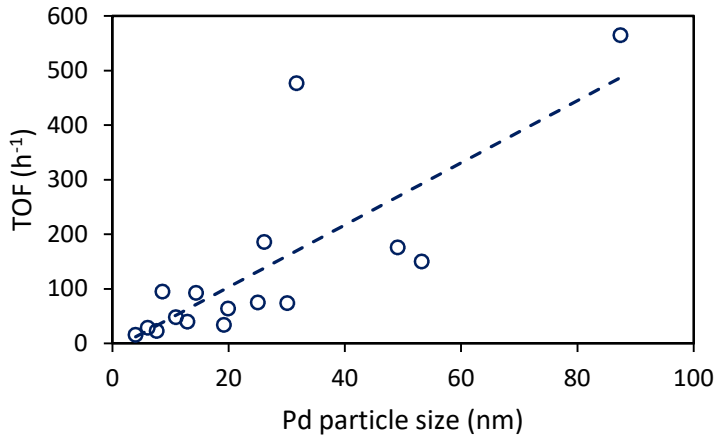

Fig. 5. Pd particle size dependency of the TOF in nitrite reduction by hydrogen on Pd/CeO_2, Pd/ZrO_2 and $Pd/Ce_xZr_{1-x}O_2$.

At longer reaction times, ammonia concentration profiles presented in Fig. 4 are characterized by a maximum which distinctly appears on Pd/CZ and Pd/CeO_2. Beyond this maximum a decline of ammonia concentration appears. It is worthwhile to note that this maximum was not observed for Pd/ZrO_2 for which the ammonia concentration tends to a plateau. Clearly, such observations underline a sequential consumption of ammonia on Pd/CZ and Pd/CeO_2. Earlier investigations already reported the occurrence of sub-reaction during the overall reduction of nitrites involving ammonia with possible reduction of nitrites by ammonium ions [22-24]. However, in most cases the conclusions are supported by weak evidences with the hypothesis that this reaction could occur in homogeneous phase. To clarify this point, the juxtaposition of Fig. 3(a) and 4(a) on 0.46Pd/CZ(EISA) can be useful. It states on a possible involvement of such a reaction. As illustrated, the consumption of ammonium ions takes

places beyond the maximum corresponding to a complete conversion of nitrites. On the basis of this observation one can rule out the involvement of a sub-reaction between nitrites and ammonium ions which rise the question on the nature of the chemical process originating the ammonia consumption. At a first glance, such evolution can be reasonably interpreted through the adsorption and/or oxidation with gas phase product emissions such as NO, N_2O or N_2 but nitrites in aqueous phase can be also considered. Fig. S3 provides quite a strong argument through the modeling the nitrite concentration in the course of nitrates reduction on bimetallic 1Pd-0.2Cu/CZ(COP) [13]. This accounts for a consecutive process. Experimental curve reveals an overproduction of nitrites assigned to ammonia oxidation. As these experiments were also performed in batch and anaerobic conditions then a point to debate is of course related to the origin of the oxidizing species involved in this process. At a first glance, the presence of trace amounts of dissolved oxygen in the reaction mixture incompletely degassed from water filtration could contribute to this process. However, such hypothesis seems to be invalidated by the absence of the sub-oxidation observed for Pd/ZrO_2. The involvement of OSC properties of $Pt/Ce_xZr_{1-x}O_2$ have been already proven in Catalytic Wet Air Oxidation [25,26]. By way of illustration, Yang et al. found a rate enhancement in the removal of succinic acid at increasing Ce concentration. Based on this, sub-oxidation could be intimately related to the surface density of active oxygen species as well as the metal-support perimeter. Indeed, electron rich neighbor metallic atoms could be capable to weaken the Ce-O bond through an electron transfer. Hence, the observations in Fig. 4 can suggest that a preferential interaction between CeO_2 or Ce-rich mixed oxide and Pd in the series Pd/CZ(COP) and Pd/CeO_2 would be more prone to oxidize ammonia. An estimation of the amount of oxygen supplied by the $Ce_xZr_{1-x}O_2$ for the re-oxidation of ammonia on 2.3Pd/CZ(COP) (~35 μmol in 50 mL) can be roughly calculated based on the H_2 consumption previously measured from temperature-programmed experiments (~2 mmol/g [14]). This corresponds to ~6.5 % of the

total oxygen amount of the support and emphasizes the fact that this sub-oxidation would be restricted to the surface and stop when all active surface and sub-surface oxygen species would be scavenged.

It is worthwhile to note that Pd/CZ(COP) and Pd/CZ(EISA) behave differently with respect to the nature of the ammonia oxidation products, especially at low Pd contents. As seen in Figure 3(b) the conversion of nitrites occurs more slowly on the Pd/CZ(COP) series than on Pd/CZ(EISA) which could be explained by an extra-production of nitrites coming from the competitive ammonia oxidation as earlier observed in Figure S4. According to this explanation, the conversion of nitrites recorded on 0.46Pd/CZ(EISA) should decrease beyond the maximum. In practice, the complete conversion still observed means that oxidation leads preferentially to gaseous products, i.e. N_2, N_2O or NO instead of nitrites. At a first glance, such difference could be partly explained by a lower surface anionic mobility of Zr-rich CZ(EISA) tetragonal structure compared to CeO_2 [18]. However, structural features as well as surface composition of the $Ce_xZr_{1-x}O_2$ support are not the unique parameters. As illustrated in Fig. 3(a) (green curves), 2.3Pd/CZ(EISA) mimics the behavior of Pd/CZ(COP) related to slower conversions and a complete conversion of nitrites delayed. These observations emphasize the fact that re-oxidation of ammonia on highly loaded Pd/CZ(EISA) can also lead to the formation of nitrites in some extent. Such observations could be associated to a deterioration of the Pd-Ce interface and higher density of metallic Pd species compared to 0.46Pd/CZ(EISA).

3.3. Kinetic modelling

A simple kinetic model depicted in Scheme 1 can be envisioned for modeling the sequential formation and consumption of ammonia through reduction and oxidation reactions. One can hypothesize a pseudo first order kinetics for nitrites reduction in agreement with earlier

investigations [27-29] which make easier the resolution of the first order differential Eqs. (1) and (5).

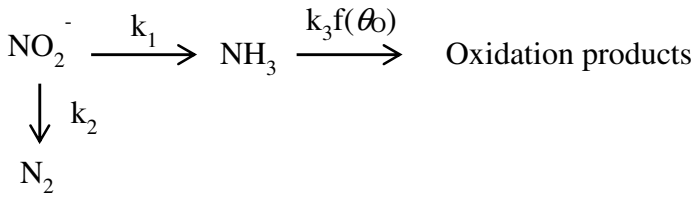

Scheme 1. Suggested parallel and sequential reactions for nitrite removal on Pd/CZ

$$\frac{d[NH_3]_t}{dt} = k_1[NO_2^-]_t - k_3 f(\theta_O)[NH_3]_t \qquad (1)$$

with $$[NO_2^-]_t = [NO_2^-]_0 \; exp \; [-(k_1 + k_2)t] \qquad (2)$$

The rate constant k_n values were estimated according to a classical least square method. The optimized rate constant values obtained when $\Sigma(r_{exp} - r_{cal})^2$ tends to a minimum are reported in Table 3. The order of magnitude for k_1+k_2 can be roughly calculated from the evolution of nitrites concentration vs. time solving Eq. (2). For ammonia consumption we have considered a pseudo rate constant which accounts for the available concentration of surface oxygen species from the support. It is worthwhile to note that the related oxygen species are not refilled under anaerobic conditions which means that this reaction is not catalytic but stoichiometric. Eq. (3) resulted from the integration of Eq. (1) is theoretically suited to model the evolution of the ammonium ion concentration vs. time.

$$[NH_3]_t = \frac{k_1[NO_2^-]_0}{k_2+k_1-k_3 f(\theta_O)} \left[exp \; [-k_3 f(\theta_O)t] - exp \; [-(k_1 + k_2)t]\right] \qquad (3)$$

The numerical values for k_1, k_2 and $k_3f(\theta_O)$ from the adjustment routine are reported in Table 3 and then compared to those obtained according to the same method on Pd/CeO_2 and Pd/ZrO_2. Starting with Pd/CZ, at increasing reduction temperature, the rate constant k_2 as well

as the sum k_1+k_2 also increase. However, these evolutions are not strictly related to significant changes of the k_2/k_1+k_2 ratio which reflects the initial selectivity to ammonia formation. The absence of any correlation between k_2 and the particle size of palladium is consistent with previous statements on a weak sensibility of the location of Pd atoms for the hydrogenation of chemisorbed N atoms. Let us now compare these values with those calculated on supported Pd on single oxides. As a general trend, all the rate constant values for Pd/CeO_2 are usually higher than that optimized for Pd/ZrO_2 which matches the slow nitrites reduction as observed in Fig. 3(c). The values almost nil for $k_3f(\theta_O)$ on Pd/ZrO_2 underline the weak lability of Zr-O quite unreactive in our experimental conditions in comparison the Ce-O bond. As exemplified in Figs. 6 and 7, a good correlation is obtained between predicted and measured ammonium ions concentrations.

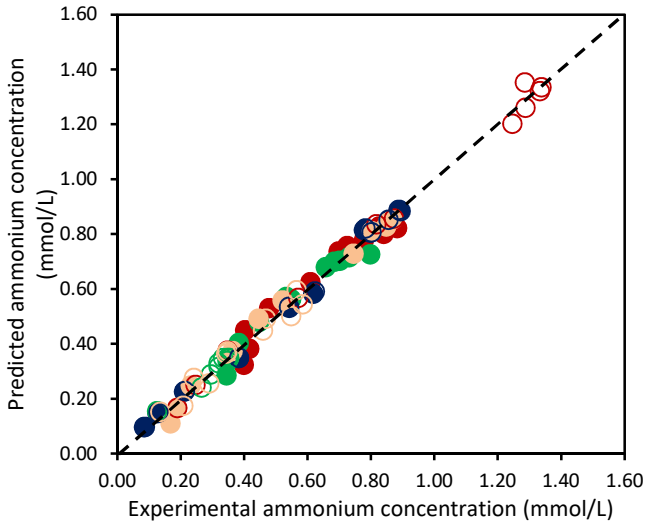

Fig. 6. Correlation between predicted and experimental concentration of ammonium ions formed during the reduction of nitrites on Pd/CZ catalysts: ● 0.46Pd/CZ(EISA)-500; ● 0.46Pd/CZ(EISA)-300; ● 2.3Pd/CZ(EISA)-500; ● 2.3Pd/CZ(EISA)-300; ○ 0.46Pd/CZ(COP)-500; ○ 0.46Pd/CZ(COP)-300; ○ 2.3Pd/CZ(COP)-500; ○ 2.3Pd/CZ(COP)-300.

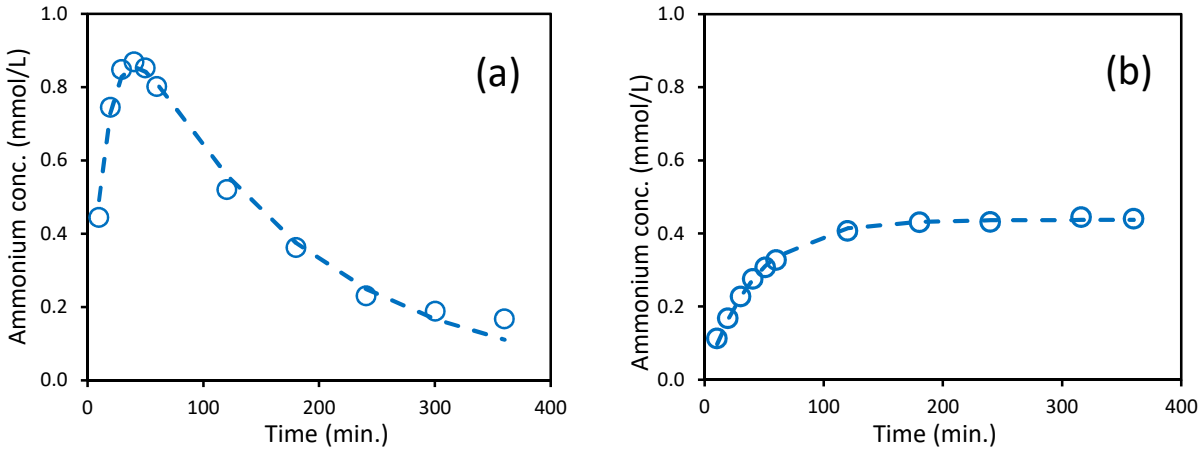

Fig. 7. Example of comparisons between predicted and experimental ammonium concentration profiles during nitrites reduction by hydrogen at 20°C in batch conditions on 2.3Pd/CZ(EISA) (a) and Pd/ZrO_2(EISA) (b) pre-reduced at 300°C.

Table 3. Rates and optimized rate constants determined on Pd supported catalysts on single and mixed ceria-zirconia oxides for the reduction of nitrites by hydrogen.

Catalyst	Pre-Red. Temp. (°C)[a]	Initial spec. Rate (mol h^{-1} g^{-1})	TOF (h^{-1})	$k_1 + k_2$ (10^{-2} min^{-1})	k_2 (10^{-2} min^{-1})	$k_3 f(\theta_O)$ (10^{-2} min^{-1})	$k_2/k_1 + k_2$	$k_3 f(\theta_O)/k_2$
2.3Pd/CZ(EISA)	300	1.2×10^{-3}	29	6.20	3.16	0.67	0.51	0.21
	500	7.8×10^{-4}	64	7.82	4.03	0.71	0.52	0.18
0.46Pd/CZ(EISA)	300	5.4×10^{-4}	95	13.17	4.74	0.29	0.36	0.06
	500	7.3×10^{-4}	477	39.87	15.63	0.27	0.39	0.02
2.3Pd/CZ(COP)	300	1.1×10^{-3}	48	0.76	0.76	1.29	1.00	1.70
	500	8.5×10^{-4}	176	7.62	3.94	0.71	0.51	0.18
0.46Pd/CZ(COP)	300	8.5×10^{-4}	34	5.78	0.92	~ 0	0.16	~ 0
	500	1.2×10^{-4}	74	6.69	5.34	0.68	0.80	0.13
2.3Pd/CeO_2(EISA)	300	1.7×10^{-3}	186	2.03	1.37	0.48	0.67	0.35
	500	6.8×10^{-4}	150	4.63	2.61	0.37	0.56	0.14
0.46Pd/CeO_2(EISA)	300	1.9×10^{-4}	16	22.63	15.70	0.67	0.70	0.04
	500	1.5×10^{-4}	40	10.41	7.37	0.80	0.71	0.11
2.3Pd/ZrO_2(EISA)	300	7.2×10^{-4}	23	2.62	0.47	0.03	0.18	0.07
	500	1.6×10^{-3}	565	2.44	0.48	~ 0	0.20	~ 0
0.46Pd/ZrO_2(EISA)	300	3.1×10^{-4}	93	2.98	0.47	~ 0	0.16	~ 0
	500	1.5×10^{-4}	75	4.72	0.52	~ 0	0.11	~ 0

[a] Temperature of the *ex situ* pre-reductive treatment under pure hydrogen flow

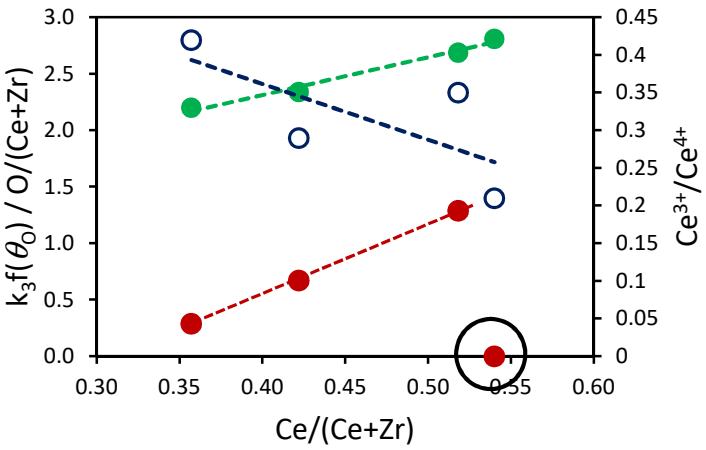

Fig. 8. Plots of $k_3f(\theta_O)$(●), Ce^{3+}/Ce^{4+} (○) and O/(Ce+Zr) (●) vs. Ce/(Ce+Zr) ratio extracted from XPS analysis on Pd/CZ pre-reduced at 300°C.

At a first glance, for the Pd/CZ samples pre-reduced at 300°C Fig. 8 shows an increase of the pseudo rate constant $k_3f(\theta_O)$ with respect to the relative cerium composition given by the Ce/(Ce+Zr) ratio (see Table 2). However, this comparison fails to describe the behavior of 0.46Pd/CZ(COP) corresponding to a predicted rate constant almost null. Jointly, $k_3f(\theta_O)$ seems to be also related to the evolution of the concentration of surface oxygen species given by the ratio O/(Ce+Zr). A weak dependency appears with the ratio Ce^{3+}/Ce^{4+} related to the concentration of the oxygen vacancies [16]. Such a lack of consistency could be related to an *in situ* reduction during the XPS measurements as already reported elsewhere under UHV conditions [30,31]. However, the weak trend observed on the ratio Ce^{3+}/Ce^{4+} still matches with that observed on O/(Ce+Zr) associated to the formation of anionic oxygen vacancies. On the basis of these comparisons, the subsequent oxidation of ammonia seems to depend on the reactivity of oxygen bonded to cerium. Nevertheless, this conclusion could be insufficient. Indeed, inaccuracies lie in the role played by palladium on the reactivity of surface oxygen species in relation to its dispersion and oxidation state.

As earlier suggested, Pd can weaken the Ce-O bond as exemplified on Pt/$Ce_xZr_{1-x}O_2$ for formic acid oxidation [20]. The length of the Pd-Ce interface could be a crucial parameter in determining the reactivity of such surface oxygen species [32]. The plots $k_3f(\theta_O)$ vs. Ce/(Ce+Zr) in Figure 9 take into account the pseudo rate constants predicted for

Pd/CeO_2(EISA) and Pd/ZrO_2(EISA) for Ce/(Ce+Zr) ratios of respectively 1 and 0. Accordingly, the juxtaposition of distinct curves for samples containing 2.3 and 0.46 wt.% Pd, reduced at 300 and 500°C, bring more insights for revealing the impact of the Pd loading, dispersion and oxidation state in relation to the temperature of the pre-reductive treatment. As already discussed the pseudo rate constant almost null recorded for Pd/ZrO_2(EISA) irrespective of the pre-reduction temperature and the metal loading reflects the poor reactivity of the surface oxygen species contrarily to Pd/CeO_2. It is worthwhile to note that higher values are obtained for $k_3f(\theta_O)$ on 2.3Pd/CZ(EISA) than on 2.3Pd/CeO_2(EISA) with a weak effect of the pre-reduction temperature. This tendency reflects the higher OSC properties of CZ(EISA) mixed oxides but also the improved reactivity of the surface oxygen due to closer interactions with highly dispersed metallic Pd species. On the contrary, $k_3f(\theta_O)$ on 0.46Pd/CZ(EISA) sample is lower than that optimized on 0.46Pd/CeO_2(EISA) exhibiting a higher Pd dispersion. A lower fraction of un-reducible oxidic Pd species less prone to weaken the Ce-O bond could be responsible of such evolution on 0.46Pd/CZ(EISA). It is remarkable that an increase of the pre-reduction temperature on this latter catalyst has a beneficial effect with an increase of $k_3f(\theta_O)$ suggesting that dual active sites composed of metallic Pd sites at the vicinity of Ce-O would be involved in ammonia oxidation. Finally, the comparison with 2.3Pd/CZ(COP) is relevant showing that this catalyst outperforms 2.3Pd/CZ(EISA) when the pre-reduction is performed at 300°C. On the other hand, a pre-reduction at 500°C has a strong detrimental effect with a sharp decrease of $k_3f(\theta_O)$ on 2.3Pd/CZ(COP) likely related to a deterioration of the Pd-Ce interface due to extensive Pd particle sintering possibly in connection with a more stronger structural heterogeneity compared to 2.3Pd/CZ(EISA).

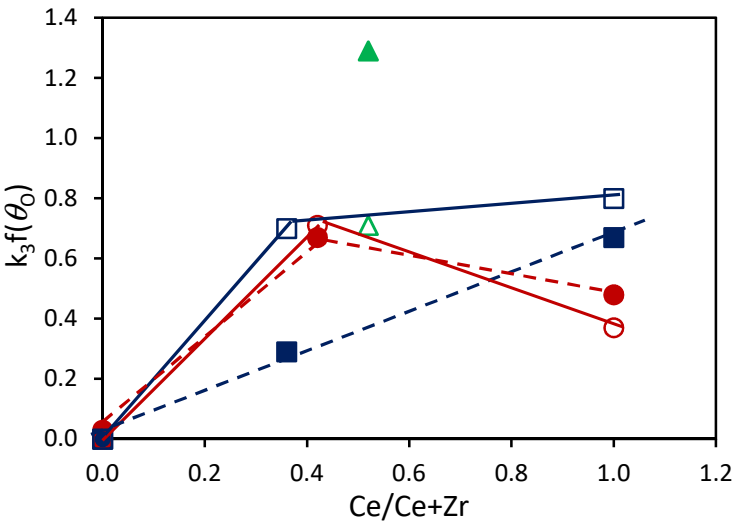

Fig. 9. Plot of $k_3f(\theta_O)$ vs. the ratio Ce/(Ce+Zr) on 2.3Pd/$Ce_xZr_{1-x}O_2$(EISA)-Red.300°C (●); 2.3Pd/$Ce_xZr_{1-x}O_2$(EISA)-Red.500°C (○); 0.46Pd/$Ce_xZr_{1-x}O_2$(EISA)-Red.300°C (■); 0.46Pd/$Ce_xZr_{1-x}O_2$(EISA)-Red.500°C (□); 2.3Pd/CZ(COP)-Red.300°C (▲); 2.3Pd/CZ(COP)-Red.500°C (△).

4. Conclusion

This study dealt with the kinetics of undesired ammonia production in the course of catalytic water denitrification over palladium supported on structured ceria-zirconia mixed oxides. Different parameters were investigated referring the influence of the preparation method upon the bulk segregation, palladium loading and the pre-reduction temperature affecting the palladium dispersion. In all cases, ammonia production occurs readily while a weak structure-sensitivity is discernible likely due to a strong support effect inducing electron-rich active metallic palladium particle which could provoke an over hydrogenation of nitrites to ammonia. Interestingly, a maximum in the concentration profiles revealed the existence of a secondary ammonia oxidation reaction. An extra oxidation of ammonia with residual nitrites has been ruled out based on the comparison with different support materials exhibiting various surface oxygen mobility and related concentration. Hence, in anaerobic conditions a stoichiometric reaction would involve reactive oxygen species bonded to ceria.

The kinetic analysis revealed a sequential process from which the exploitation of concentration profiles of ammonia vs. time led to the estimation of the rate constants, especially of those related to the oxidation of ammonia which has been found dependent on

the oxygen coverage and on the Pd-Ce interface which can be modulated according to the Pd loading and the pre-reduction temperature. Regarding this specific re-oxidation of ammonia and especially the evolution observed on the pseudo rate constant $k_3 f(\theta_O)$, the best compromise seems to be obtained on pre-reduced 2.3Pd/CZ(COP) pre-reduced at 300°C. On the other hand, a pre-reduction at higher temperature has a strong detrimental effect inducing a significant decrease of the rate constant $k_3 f(\theta_O)$ whereas a weak sensibility is noticeable on 2.3Pd/CZ(EISA) emphasizing the peculiar structural properties of the support and the related preparation method to stabilize the Pd-Ce interface.

Acknowledgments

The authors would like to thank the CNRS through the Project research PICS : N°286849 "NanoCat" and greatly acknowledge the financial support from the CCIFER – ANCS and the French Embassy (PhD fellowship awarded to S. Troncéa who won the competition *« Graine de Chercheur et Energie Durable »*). Chevreul Institute (FR 2638), Ministère de l'Enseignement Supérieur et de la Recherche, Région Nord – Pas de Calais and FEDER are acknowledged for supporting and funding partially this work.

References

1. L.J. Puckert, Environ. Sci. Technol. 29 (1995) 408A–414A.
2. K. Reddy, Water Res. 34 (2000) 995–1001.
3 Y.N. Kim, M.Y. Kim, M. Choi, Chem. Eng. J. 289 (2016) 423–432.
4. J.K. Chinthaginjala, L. Lefferts, Appl. Catal. B 101 (2010) 144–149.
5. F. Epron, F. Gauthard, C. Pinéda, J. Barbier, J. Catal. 198 (2001) 309–318.
6. Y. Matatov-Meytal, V. Barelko, I. Yuranov, L. Kiwi-Minsker, A. Renken, M. Sheintuch, Appl. Catal. B 31 (2001) 233–240.
7. F. Zhang, S. Miao, Y. Yang, X. Zhang, J. Chen, N. Guan, J. Phys. Chem. C 112 (2008) 7665–7671.
8 Y. Yoshinaga, T. Akita, I. Mikami, T. Okuhara, J. Catal. 207 (2002) 37–45.
9. F. Epron, F. Gauthard, J. Barbier, J. Catal. 206 (2002) 363–367.
10. M.S. Kim, D.W. Lee, S.H. Chung, J.T. Kim, I.H. Cho, K.Y. Lee, J. Mol. Catal. A, 2014, 392, 308–314.
11. C.P. Theologides, G.G. Olympiou, P.G. Savva, K. Kapnisis, A. Anayisotos, C.N. Costa, Appl. Catal. B 205 (2017) 443–454.
12. U. Prüsse, K.-D. Vorlop, J. Mol. Catal. A 173 (2001) 313–328.

13. P. Granger, S. Troncéa, J.P. Dacquin, M. Trentesaux, O. Gardoll, N. Nuns, V.I. Parvulescu, Appl. Catal. B 253 (2019) 391–400.
14. P. Granger, S. Troncéa, J.P. Dacquin, M. Trentesaux, V.I. Parvulescu, Applied Catalysis B 224 (2018) 648–659.
15. B. Zhao, G.F. Li, C.H. Ge, Q.Y. Wang, R.X. Zhou. Appl. Catal. B 96 (2010) 338–349.
16. P. Esteves, Y. Wu, C. Dujardin, M.K. Dongare, P. Granger, Catal. Today 176 (2011) 453–457.
17. P. Fornasiero, J. Kaspar, M. Graziani, J. Catal. 167 (1997) 576–580.
18. S.A. Ghom, C.Z. Zamani, S. Nazarpour, T. Andreu, J.R. Morante, Sensors and Act. B 140 (2009) 216–221.
19. Q. Wang, M. Yue, Q. Zhong, M. Cui, X. Huang, Y. Hou, L. Wang, Y. Yang, Z. Long, Z. Feng, J. Rare Earths 34 (2016) 695–702.
20. M.-S. Kim, S.-H. Chung, C.J. Yoo, M.S. Lee, I.-H. Cho, D.-W. Lee, K.-Y. Lee, Appl. Catal. B 142–143 (2013) 354–361.
21. J. Lee, Y.G Hur, M.-S. Kim, K.-Y. Lee, J. Mol. Catal. A 399 (2015) 48–52.
22. B. Ileri, O. Ayyildiz, O. Apaydin, J. Hazard. Mater. 292 (2015) 1–8.
23. D.K. Lee, J.S. Cho, W.L. Yoon, Chemosphere 61 (2005) 573–578.
24. G. Lafaye, J. Barbier Jr., D. Duprez, Catal. Today 253 (2015) 89–98.
25. S. Yang, M. Besson, C. Descormes, Appl. Catal. B 100 (2010) 282–288.
26. S. Keav, A. Espinoza de los Monteros, J. Barbier Jr., D. Duprez, Appl. Catal. B 150-151 (2014) 402–410.
27. A.M.E. Khalil, O. Eljamal, S. Jribi, N. Matsunaga, Chem. Eng. J. 287 (2016) 367–380.
28. G.C.C. Yang, H.L. Lee, Water Research 39 (2005) 884–894.
29. Z. Zhang, Z. Hao, Y. Yang, J. Zhang, Q. Wang, X. Xu, Desalination 257 (2010) 158–162.
30. M. Piumetti, S. Bensaid, N. Russo, D. Fino, Appl. Catal. B 180 (2016) 271–282;
31. E.C. Lovell, J. Horlyck, J. Scott, R. Amal, Appl. Catal. A 546 (2017) 47–57.
32. J. Chen, Y. Wu, W. Hu, P. Qu, G. Zhang, P. Granger, L. Zhong , Y. Chen Appl. Catal. B 264 (2020) Article 118475.

Graphical Abstract

Overall reduction process of nitrites